

# A point process approach to assess the frequency dependence of ultrasound backscattering by aggregating red blood cells

David Savéry and Guy Cloutier<sup>a)</sup>

Laboratory of Biomedical Engineering, Clinical Research Institute of Montréal, 110 Avenue des Pins Ouest, Montréal, Québec H2W 1R7, Canada and Laboratory of Biorheology and Medical Ultrasonics, University of Montréal Hospital, Québec, Canada

(Received 29 December 2000; accepted for publication 9 September 2001)

To study the shear-thinning rheological behavior of blood, an acoustical measurement of the erythrocyte aggregation level can be obtained by analyzing the frequency dependence of ultrasonic backscattering from blood. However, the relation that exists among the variables describing the aggregation level and the backscattering coefficient needs to be better clarified. To achieve this purpose, a three-dimensional random model, the Neyman–Scott point process, is proposed to simulate red cell clustering in aggregative conditions at a low hematocrit ( $H < 5\%$ ). The frequency dependence of the backscattering coefficient of blood, in non-Rayleigh conditions, is analytically derived from the model, as a function of the size distribution of the aggregates and of their mass fractal dimension. Quantitative predictions of the backscatter increase due to red cell aggregation are given. The parametric model of backscatter enables two descriptive indices of red cell aggregation to be extracted from experimental data, the packing factor  $W$  and the size factor  $\Delta$ . Previously published backscatter measurements from porcine whole blood at 4.5% hematocrit, in the frequency range of 3.5 MHz–12.5 MHz, are used to study the shear-rate dependence of these two indices.

© 2001 Acoustical Society of America. [DOI: 10.1121/1.1419092]

PACS numbers: 43.80.Cs, 43.80.Jz, 43.35.Bf [FD]

## LIST OF SYMBOLS

$a$	mean radius of the red blood cells	$m$	number density
$B$	a compact set of points	$m_0$	number density of the aggregates
$c$	speed of sound	$N(\mathbf{x})$	local microscopic density
$\bar{C}$	relative impedance mismatch between red cells and plasma	$N_c, N_c(i)$	random numbers of particles per aggregate
$D$	mass fractal dimension	$n_c$	mean number of particles per aggregate, $E[N_c]$
$\Delta$	size factor	$d\Omega$	solid angle of observation relatively to the scattering volume
$\delta$	Dirac $\delta$ -function	$P$	probability
$E[A]$	mathematical expected value of a random variable $A$	$dP$	power of the backscattered wave in $d\Omega$
$f, f_0, f_i$	frequencies	$\mathbf{q}$	scattering vector ( $-2\mathbf{k}$ for backscattering)
$f_X(\mathbf{x})$	probability density function of $\mathbf{X}$	$\mathbf{r}$	spatial position of the observer
$\Phi$	eigenvectors matrix of the covariance matrix $E[\mathbf{X}^T\mathbf{X}]$	$\rho_0$	mass density
$g(\mathbf{r})$	pair-correlation function	$S(\mathbf{q})$	structure factor $= (1/M)  \sum_i \exp(-j\mathbf{q} \cdot \mathbf{x}_i) ^2$
$H$	hematocrit	$\Sigma$	diagonal matrix of the eigenvalues of the covariance matrix $E[\mathbf{X}^T\mathbf{X}]$
$I$	identity matrix	$\sigma$	standard deviation of $\mathbf{X}$ when $\mathbf{X}$ is isotropic
$I_{\text{incident}}$	intensity of the incident pressure wave	$\sigma_b(-2\mathbf{k})$	backscattering cross-section
$j$	$\sqrt{-1}$	$\sigma_c$	standard deviation of $N_c$ , $\sigma_c^2 = E[N_c^2] - E[N_c]^2$
$J(W, \Delta)$	quadratic error to minimize for nonlinear regression	$A^T$	transposition of a matrix $A$
$J_{\text{min}}$	minimal value of $J(W, \Delta)$	$V_s$	volume of the particle
$\mathbf{k}, \mathbf{k}_i$	incident wave vectors	$V_B$	volume of the compact set $B$
$\chi(\mathbf{k})$	backscattering coefficient	$dV$	scattering volume
$\kappa_0$	compressibility	$W$	packing factor $= \lim_{q \rightarrow 0} S(\mathbf{q})$
$l_{\text{cor}}$	correlation length	$X = \{\mathbf{x}_i\}_{i=1 \dots M}$	set of the random positions of the red blood cells
$\lambda$	wavelength	$\mathbf{X}$	random position of a red cell inside a centered aggregate
$M$	total number of particles	$X_{il}$	position of the $l$ th particle inside the $i$ th aggregate
		$\mathbf{x}$	position within the scattering volume

<sup>a)</sup>Electronic mail: guy.cloutier@umontreal.ca

$Y = \{Y_i\}$  set of the random positions of the centers of aggregates  
 $Z_p$  acoustical impedance of the particle

$Z_0$  mean acoustical impedance  
 $Z_X(B)$  random number of particles of  $X$  falling into the compact set  $B$

## I. INTRODUCTION

Blood is a complex tissue to characterize by ultrasonic means because of its heterogeneous structure. Blood interacts with acoustic waves because of the presence of cells flowing in the plasma (99% are red cells) that scatter ultrasound nonisotropically. The high density of red cells (their volumic fraction reaches about 45%) and their ability to form reversible aggregates under the cumulative effects of chemical, physical and hydrodynamic interactions create intricate spatial structures that influence the scattering properties of blood.

Clinically, the purpose of blood characterization by ultrasound is to offer the possibility of investigating *in vitro* and *in vivo* the rheological attributes of blood. The viscoelasticity and the thixotropy of blood strongly depend on the formation and disruption of red blood cell aggregates and any disturbance in these mechanical parameters can alter the micro and macrocirculation by initiating stasis zones, enhancing thrombus formation, and favoring tissue ischemia.<sup>1</sup> It would consequently be relevant to assess *in vivo* the hemorheological disorders of patients and to take them into account in conventional cardiovascular risk profiles.<sup>2</sup>

Classical tissue characterization techniques consist of finding the frequency dependence of attenuation and backscatter properties of the material and using them as acoustical indicators of the underlying microstructure. This was proven useful to detect diseased tissues in several clinical applications. Infarcted myocardium,<sup>3</sup> atherosclerotic carotid arteries<sup>4</sup> or cirrhotic livers<sup>5</sup> were shown to have scattering properties that differ from their healthy counterparts. Spectral characterization of blood backscattering has already been performed experimentally<sup>6-8</sup> and has shown sensitivity to the microstructural packing state of the red blood cells.

Theoretical efforts have been made to elucidate the relation between the backscattering properties of blood, usually quantified by the value of the backscattering coefficient, and the frequency of the incident wave, the hematocrit, the flow condition (steady state or turbulent), or the red cell aggregation level.<sup>9-13</sup> Twersky<sup>9</sup> proposed a parameter called packing factor to describe the backscattering coefficient of a distribution of hard particles. The primary assumption of this theory is that the spatial scale of the inhomogeneities in acoustical impedance must be much smaller than the acoustical wavelength.

This approximation succeeds to explain the hematocrit dependence of the backscattering by nonaggregating suspensions of red cells but fails to predict the frequency dependence observed in experimental conditions when red cell aggregation is significant. As the packing factor is independent on the frequency, the backscattering coefficient is expected to increase linearly with the fourth power of the frequency<sup>14</sup> in the low frequency approximation. However Yuan and Shung,<sup>6</sup> Foster *et al.*,<sup>7</sup> and Van der Heiden *et al.*<sup>8</sup> observed

that the frequency dependence of blood is lower when the flow rate is decreased, and thus when the aggregation is enhanced for frequencies as low as 3.5 MHz.

These results suggest that the theoretical understanding of blood scattering at higher frequencies is incomplete. We propose to generalize the packing factor theory for higher frequencies by introducing the frequency-dependent structure factor. It is intended to use it as a spectral signature of the aggregation process that is more relevant for ultrasonic characterization than a single measurement at a low frequency.

The purpose of this study was to predict the frequency dependence of the backscattering coefficient from blood characterized by different levels of red blood cell aggregation. It is hypothesized that the spatial pattern formed by the aggregates of red cells governs the backscattering strength of blood. Red cell positioning is modeled as a random spatial point-process and it is considered that red cell aggregation modifies the statistical parameters of this random phenomenon. The Neyman-Scott process (NSP) gives a random framework that is convenient for the analytical derivation of the backscattering coefficient. In this paper, the method used to theoretically predict the backscattering coefficient of a weak scattering suspension is described in Sec. II, then the NSP is introduced in Sec. III to model red cell aggregation and to derive the analytical expression of the backscattering properties of blood. In Sec. IV, results on the predicted effects of red cell aggregation on the backscattering coefficient are given, and the question of inferring descriptive aggregation parameters using experimental backscatter data is discussed.

## II. SCATTERING BY A SUSPENSION OF WEAK SCATTERERS

### A. Decomposition of the backscattering coefficient

The propagation of an acoustic wave into a linear medium depends on the spatial distribution of density  $\rho_0(\mathbf{x})$  and compressibility  $\kappa_0(\mathbf{x})$ , where  $\mathbf{x}$  represents the spatial position. When these spatial functions are precisely known, the wave equation can be theoretically solved once the source parameters are given, and conveys the relation between the pressure measured at the surface of the receiver and the various acoustic properties of the medium. In a heterogeneous medium like blood, it would be difficult to describe accurately the exact spatial distributions of density and compressibility. This is why the propagation medium is seen, in this article, as a realization of a random process which can be characterized by statistical mean parameters that depict its macroscopical properties. Measurement of the backscattering properties of a sample of this material should provide clues on the value of these mean parameters as shown in this section.

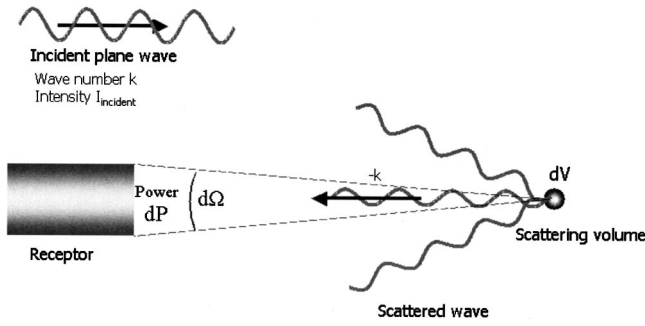


FIG. 1. Scattering experiments and symbols.

In this paper, we assume that an ideal backscattering experiment (Fig. 1) consists of the insonification of a material volume  $dV$  by a monochromatic pressure plane wave of intensity  $I_{\text{incident}}$  and by the measurement of the power  $dP$  of the backscattered wave into a small solid angle  $d\Omega$ . The result is expressed in normalized terms ( $\text{m}^{-1}\text{sr}^{-1}$ ) by the differential backscattering coefficient. If the incident plane wave has a wave vector  $\mathbf{k}$  ( $|\mathbf{k}| = 2\pi/\lambda$ ,  $\lambda$  being the wavelength), the (differential) backscattering coefficient  $\chi(\mathbf{k})$  is defined by:

$$\chi(\mathbf{k}) = \frac{dP}{I_{\text{incident}} d\Omega dV}. \quad (1)$$

The fluctuations in density and compressibility within blood are supposed small enough to hypothesize that the Born approximation is valid. We also assume that the medium  $dV$  is composed of  $M = m dV$  identical spherical particles whose centers are positioned in  $\{\mathbf{x}_i\}_{i=1\dots M}$ ,  $m$  being the number density of the particles. The  $M$  particles are embedded in a homogeneous medium (like the plasma) with a mean characteristic acoustical impedance  $Z_0$ .

These hypotheses allow to write the backscattering coefficient in the known factorized form:<sup>9</sup>

$$\chi(\mathbf{k}) = mS(-2\mathbf{k})\sigma_b(-2\mathbf{k}). \quad (2)$$

In Eq. (2) are introduced the structure factor  $S(\mathbf{q}) = (1/M)|\sum_{i=1}^M e^{-j\mathbf{q}\cdot\mathbf{x}_i}|^2$ , function of the scattering vector  $\mathbf{q} = -2\mathbf{k}$ , and the backscattering cross-section of the individual scatterer  $\sigma_b(-2\mathbf{k})$ .

For weak scattering spherical particles of radius  $a$  and volume  $V_s = \frac{4}{3}\pi a^3$ , the backscattering cross-section is given by:<sup>15</sup>

$$\sigma_b(-2\mathbf{k}) = \frac{1}{4\pi^2} V_s^2 \bar{C}^2 k^4 \left( 3 \frac{\sin(2ka) - 2ka \cos(2ka)}{(2ka)^3} \right)^2, \quad (3)$$

where  $\bar{C} = (Z_p - Z_0)/Z_0$  is the small relative mismatch between  $Z_p$ , the particle impedance, and  $Z_0$ .

Equation (2) exhibits the expected result that the scattering strength of a tissue depends on the intrinsic acoustical properties of the scatterers, described by the backscattering cross-section  $\sigma_b(-2\mathbf{k})$ , and also on the spatial positioning of particles whose second order statistics are described by the structure factor  $S(\mathbf{q})$ . The aggregation phenomenon is supposed to only affect the structure factor, as red cell properties and hematocrit remain constant in the sample macroscopical volume.

## B. Pair-correlation function of a point process and structure factor

The structure factor  $S(\mathbf{q})$  can be influenced in a complex way by the hematocrit  $H$ , the geometric dimension of the particle and also by the physical factors governing the aggregation process. To theoretically estimate variations of the structure factor, the positioning of the scatterers in the medium is considered as a realization of a random point process, that obeys a random model with average parameters characterizing the aggregation level. Theoretically, a point distribution can be described by its microscopic density  $N(\mathbf{x})$ :

$$N(\mathbf{x}) = \sum_{i=1}^M \delta(\mathbf{x} - \mathbf{x}_i), \quad (4)$$

where  $\delta$  is the Dirac  $\delta$ -function and  $X = \{\mathbf{x}_i\}_{i=1\dots M}$  are considered as random positions of the scatterers. Writing  $\hat{N}(\mathbf{q}) = \int N(\mathbf{x}) e^{-j\mathbf{q}\cdot\mathbf{x}} d\mathbf{x}$  the Fourier transform of the microscopic density, the mean structure factor can be derived from the mean energy spectrum of  $N(\mathbf{x})$  by:

$$S(\mathbf{q}) = \frac{E[|\hat{N}(\mathbf{q})|^2]}{M}, \quad (5)$$

where  $E[\ ]$  represents the expected value of a random variable. The pair-correlation function

$$g(\mathbf{r}) = \frac{P(\mathbf{x} \in X \text{ and } \mathbf{x} + \mathbf{r} \in X)}{P(\mathbf{x} \in X)P(\mathbf{x} + \mathbf{r} \in X)},$$

can be related to the structure factor. Writing  $E[N(\mathbf{x})N(\mathbf{x} + \mathbf{r})] = m^2 g(\mathbf{r}) + m \delta(\mathbf{r})$ , one derives<sup>9</sup> for  $\mathbf{q} \neq \mathbf{0}$ :

$$S(\mathbf{q}) = 1 + m \int (g(\mathbf{r}) - 1) e^{-j\mathbf{q}\cdot\mathbf{r}} d\mathbf{r}. \quad (6)$$

This formula shows that variations of the pair-correlation function induced by changes in the spatial organization of the red cells will directly affect the structure factor and the scattering properties of blood.

## C. Correlation length and corresponding scattering regimes

Depending on the relative values of the correlation length  $l_{\text{cor}}$ , defined by  $|\mathbf{r}| > l_{\text{cor}} \Rightarrow g(\mathbf{r}) = 1$ , and of the wavelength  $\lambda$ , two different aggregation regimes can be distinguished. This correlation length can be roughly seen as the diameter of the clusters present in the medium.

### 1. Rayleigh scattering

When  $l_{\text{cor}} \ll \lambda$ , we have the low frequency approximation that leads to the definition of the *packing factor*  $W$ , the zero-frequency limit of the structure factor. This happens when scatterers are aggregated in clusters much smaller than the wavelength. In this case,

$$\lim_{q \rightarrow 0} S(\mathbf{q}) = W = 1 + m \int (g(\mathbf{r}) - 1) d\mathbf{r}, \quad (7)$$

and

$$\chi(k) = mW\sigma_b(-2k) \approx \frac{1}{4\pi^2} HWV_s \bar{C}^2 k^4. \quad (8)$$

A medium with uncorrelated particles, corresponding to  $l_{\text{cor}} \approx 0$  has thus a unit packing factor. A low hematocrit ( $H < 5\%$ ) suspension of nonaggregating red blood cells can be approximated by such a model. The packing factor can be seen as a corrective factor that takes into account the correlations between positions of scatterers. The variations of the packing factor with the hematocrit, polydispersity and shape of hard particles have been theoretically studied by Twersky.<sup>9,16</sup> For nonaggregating particles,  $W$  tends toward 1 when the hematocrit  $H$  is low, and vanishes when  $H$  is close to 100%, because, in this case, heterogeneities giving birth to scattering no longer exist in the medium. The peak of low frequency backscattering, that arises when  $HW$  is maximal, occurs for  $H_{\text{max}} \approx 13\%$  for nonaggregating spheres but can vary with the shape of the scatterers or with the polydispersity of the distribution.<sup>16</sup>

By definition,  $W$  does not depend on the frequency. This low frequency approximation can thus only consider the fourth power frequency dependence ( $k^4$ ) of the backscattering coefficient in the Rayleigh scattering regime.

## 2. Non-Rayleigh scattering and aggregation

At least two situations can provoke the irrelevance of the low frequency approximation: either when the acoustical frequency is increased (to obtain a better spatial resolution) or when the aggregation level is so elevated that the correlation length  $l_{\text{cor}}$  becomes non-negligible compared to the wavelength. One can test the validity of these assumptions by estimating the frequency dependence of the backscattering coefficient, which should be proportional to  $k^4$  under Rayleigh conditions.

Frequency dependencies of the backscattering coefficient of whole blood as low as  $k^{1.3}$  (in the frequency range of 22–37 MHz,<sup>8</sup> at a shear rate under  $1 \text{ s}^{-1}$ ) or  $k^{0.4}$  (in the range 30–70 MHz,<sup>7</sup> at a shear rate of  $0.16 \text{ s}^{-1}$ ) have been reported in the literature. This shows that the Rayleigh approximation is inappropriate to study scattering from aggregating red cells as a function of the frequency. A particular random spatial point process, the Neyman–Scott process (NSP), is proposed to predict the effect of aggregation on the backscatter data and to clarify the relation between the frequency and the backscattering coefficient.

## III. MODELING OF RED CELL AGGREGATION BY THE NEYMAN–SCOTT PROCESS

### A. Random point processes

We consider that the set of positions  $X = \{\mathbf{x}_i\}_{i=1..M}$  of the particle centers is the realization of a random spatial process,  $M$  being either constant or a random variable such as  $E[M] = m dV$ . To fully characterize a point process, one can specify<sup>17</sup> the random numbers  $Z_X(B)$  of points falling into a compact set  $B$  included in  $dV$ . The process of aggregation is supposed locally stationary in the sample volume, which implies that the random variable  $Z_X(B)$  depends only on the shape of  $B$  and not on the position of its center. The pair-

correlation function can simply be seen as a second order property, when  $B$  is the pair of points  $\{\mathbf{x}, \mathbf{x} + \mathbf{r}\}$ :

$$g(\mathbf{r}) = \frac{P(\mathbf{x} \in X \text{ and } \mathbf{x} + \mathbf{r} \in X)}{P(\mathbf{x} \in X)^2} = \frac{1 - 2P(Z_X(\{\mathbf{x}\}) = 0) + P(Z_X(\{\mathbf{x}, \mathbf{x} + \mathbf{r}\}) = 0)}{[1 - P(Z_X(\{\mathbf{x}\}) = 0)]^2}. \quad (9)$$

$X$  is said to be a Poisson process with number density  $m$  when  $Z_X(B)$  is a Poisson random variable with mean value  $mV_B$ ,  $V_B$  being the volume of  $B$ . In this case, Eq. (9) with  $P[Z_X(B) = 0] = e^{-mV_B}$  gives  $g(\mathbf{r}) = 1$ . No spatial structure exists in the Poisson point process as the correlation length is zero, and this is why a Poisson point process can be described as a complete random distribution. The evaluation of the structure factor gives, at all frequencies,  $S(\mathbf{q}) = 1$ . A stationary Poisson point process thus cannot be an appropriate model to simulate clusters of scatterers as encountered in certain red cell aggregation conditions.

### B. The Neyman–Scott point process

The Neyman–Scott process is a random point process commonly used to model clusters of points. This random model efficiently described different statistical spatial data such as the positioning of trees in the forest,<sup>18</sup> the distribution of precious stones in soil<sup>19</sup> or the patterns of rainfall cells.<sup>20</sup>

The red cells are supposed to be grouped in clusters having random features obeying the same probability law. We intend to characterize aggregate morphology by a small number of geometrical quantities taken as aggregation indices. However, the relation between the different physical interactions involved in the aggregation process (hydrodynamics, depletion or bridging effects of the plasmatic macromolecules, electrostatic forces) and the microstructural factors defining the configurations of erythrocyte clusters will not be directly modeled, as we only want to geometrically describe the aggregation level.

The basis of a realization of an NSP lies on a Poisson process  $Y$  with a number density  $m_0$ . Each point  $Y_i$  is the center of the  $i$ th cluster surrounded by a random number  $N_c(i)$  of points, sampled from a random variable  $N_c$ . To construct this cluster,  $N_c(i)$  independent realizations  $\{\mathbf{X}_{il}\}_{l=1..N_c(i)}$  of a random vector  $\mathbf{X}$  are generated, and the  $N_c(i)$  points  $Y_i + \mathbf{X}_{il}$  compose the cluster. The microscopic density  $N(\mathbf{x})$  can then be written as:

$$N(\mathbf{x}) = \sum_i \sum_{l=1}^{N_c(i)} \delta(\mathbf{x} - Y_i - \mathbf{X}_{il}). \quad (10)$$

The parameters needed to fully describe the NSP are thus:

- (1) the number density  $m_0$  of the centers of clusters  $\{Y_i\}$ ,
- (2) the discrete probability density function  $P(N_c = n)$  of the random number  $N_c$  of points per cluster,
- (3) the spatial probability density function  $f_X(\mathbf{x})$  of the random vector  $\mathbf{X}$  (with mean 0), that characterizes the cluster size.

The characteristic function and the two first moments of the discrete distribution  $Z_{\text{NSP}}(B)$  have already been computed<sup>17</sup> as a function of the moments of  $N_c$  ( $n_c = E[N_c]$  and  $\sigma_c^2 = \text{Var}[N_c]$ ), of  $f_X(\mathbf{x})$  and of the shape of  $B$ . The number density  $m$  equals  $m_0 n_c$  and the pair-correlation function  $g(\mathbf{r})$  can be determined and is given by:

$$g(\mathbf{r}) = 1 + \frac{1}{m} \left( \frac{\sigma_c^2}{n_c} + n_c - 1 \right) \int f_X(\mathbf{x}) f_X(\mathbf{x} + \mathbf{r}) d\mathbf{x}. \quad (11)$$

According to Eq. (6), the structure factor can also be derived by computing the Fourier transform of  $g(\mathbf{r}) - 1$ :

$$S(\mathbf{q}) = 1 + \left( \frac{\sigma_c^2}{n_c} + n_c - 1 \right) \left| \int f_X(\mathbf{x}) e^{-j\mathbf{q} \cdot \mathbf{x}} d\mathbf{x} \right|^2. \quad (12)$$

### C. Aggregation parameters

The random spatial probability density  $f_X(\mathbf{x})$  physically characterizes the spatial dimension of the clusters by determining the dispersion of the red cells around the center of an aggregate. We consider here the simplest random vector distribution to model  $f_X(\mathbf{x})$ , i.e., the Gaussian model with zero mean and covariance matrix  $E[\mathbf{X}^T \mathbf{X}] = \Phi^T \Sigma \Phi$ . The diagonal matrix  $\Sigma$  represents the spatial standard deviations in the principal axes, and the orthogonal matrix  $\Phi$  is the matrix of the unitary principal axes  $\{\mathbf{e}_1, \mathbf{e}_2, \mathbf{e}_3\}$  of the clusters. An anisotropic shape of the clusters would result in different eigenvalues  $\{\sigma_1^2 \geq \sigma_2^2 \geq \sigma_3^2\}$  of the covariance matrix  $E[\mathbf{X}^T \mathbf{X}]$ . On the contrary, if the clusters are isotropic, the covariance matrix takes a simple spherical form:  $E[\mathbf{X}^T \mathbf{X}] = \sigma^2 I$ , where  $I$  is the identity matrix.

The structure factor can then be analytically computed by using Eq. (12):

$$S(\mathbf{q}) = 1 + \left( \frac{\sigma_c^2}{n_c} + n_c - 1 \right) \exp[-(\Phi \mathbf{q})^T \Sigma (\Phi \mathbf{q})]. \quad (13)$$

If the clusters are isotropic, the pair-correlation function and the structure factor have a simpler expression:

$$g(\mathbf{r}) = 1 + \frac{1}{4\pi^{3/2} m \sigma^3} \left( \frac{\sigma_c^2}{n_c} + n_c - 1 \right) \exp[-2^{-3/2} |\mathbf{r}|/\sigma^2], \quad (14)$$

and

$$S(\mathbf{q}) = 1 + \left( \frac{\sigma_c^2}{n_c} + n_c - 1 \right) \exp[-|\sigma \mathbf{q}|^2]. \quad (15)$$

To link the spatial standard deviation  $\sigma$ , related to the gyration radius of the clusters, to the first two moments  $\{n_c, \sigma_c^2\}$  of  $N_c$ , a fractal-like behavior is assumed by writing:<sup>21</sup>

$$\sigma/a = (n_c - 1)^{1/D}. \quad (16)$$

The fractal dimension  $D$  morphologically characterizes the growth process of the aggregates. Linear aggregates as the rouleaux have a fractal dimension close to 1, whereas compact spherical aggregates have a greater fractal dimension close to 3. As an isotropic model was adopted in the current study,  $D$  is related to the packing compactness of the

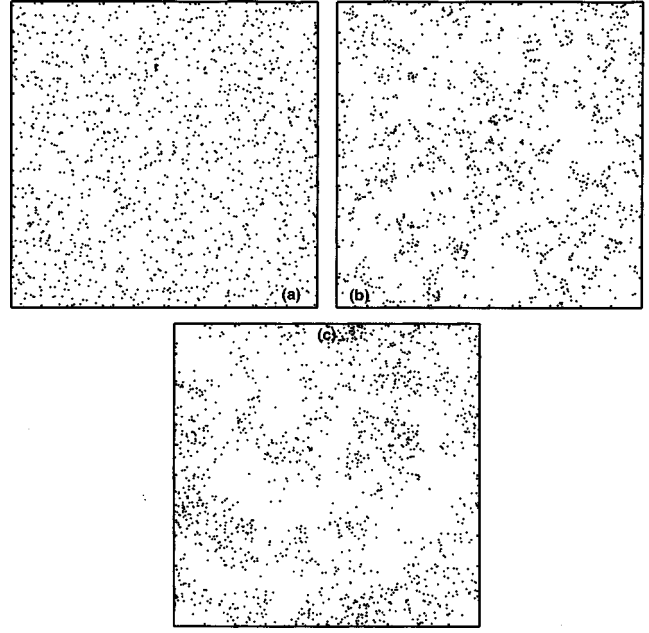


FIG. 2. 2D realizations of a Neyman-Scott model in a unit window.  $H = 0.4$ ,  $a = 0.01$ ,  $D = 2$ .  $N_c$  is uniformly taken between 1 and  $2n_c - 1$ , where (a)  $n_c = 1$ , (b)  $n_c = 5$ , (c)  $n_c = 15$ .

aggregates. The distance between particles of the same cluster tends to decrease when  $D$  increases.

Combination of Eq. (15) and Eq. (16) yields the expression of the Gaussian isotropic structure factor:

$$S(\mathbf{q}) = 1 + (W - 1) \exp\left(-\frac{|a\mathbf{q}|^2}{2\Delta^2}\right). \quad (17)$$

Two nondimensional aggregation parameters,  $W$ , the packing factor, and  $\Delta$ , a size factor, contribute to  $S(\mathbf{q})$ :

- (1)  $W = n_c + (\sigma_c^2/n_c)$  increases when the number of cells per aggregate grows.  $W$  can be seen as an indicator of the size of aggregates in terms of *number* of cells per aggregate.  $W$  is the limit of the structure factor when the incident frequency tends toward zero.
- (2)  $\Delta = (1/\sqrt{2})(n_c - 1)^{-1/D} = a/(\sqrt{2}\sigma)$  decreases when the spatial dimension of the cluster increases. This index  $\Delta$  is related to the *spatial* extent of the clusters and controls the rate of decrease of the structure factor between  $W$  and 1, when varying the incident frequency.

Figure 2 illustrates spatial patterns generated by the NSP. Three 2D realizations (2D simulations are here shown for convenience but all results presented in the rest of the paper are three-dimensional) are shown in a unit window with  $H = 0.4$ ,  $a = 0.01$ ,  $D = 2$ , and with  $N_c$ , taken as a random integer uniformly distributed between 1 and  $2n_c - 1$ , with  $n_c = 1, 5$  and 15. Table I gives the packing factors and the size factors corresponding to these configurations.

### D. Analytical formulation of the backscattering coefficient

By substituting Eqs. (17) and (3) into Eq. (2), and noting that  $m = H/V_s$ , one obtains the backscattering coefficient of

TABLE I. Values of the packing factor and of the size factor for the 2D simulations shown in Fig. 2. The fractal dimension is  $D=2$ .

$n_c$	$W$	$\Delta$	$\sigma/a$
1	1	$+\infty$	0
5	6.3	0.35	2
15	19.7	0.19	3.7

a medium composed of weak scattering spherical particles with an arrangement described by an isotropic Gaussian Neyman–Scott model:

$$\chi^{\{W,\Delta\}}(k) = \frac{1}{3\pi a} H \bar{C}^2(ka)^4 \left[ 3 \frac{\sin 2ka - 2ka \cos 2ka}{(2ka)^3} \right]^2 \times (1 + (W-1)e^{-2(ka)^2/\Delta^2}). \quad (18)$$

#### IV. RESULTS AND DISCUSSION

Because of the variations of the structure factor with the packing factor  $W$  and the size factor  $\Delta$ , the backscattering coefficient of blood varies with the morphology of the red cell aggregates. Depending on the range of frequencies studied, the sensitivity of the backscattering coefficient to changes in aggregation properties can also vary. The proposed model allows to evaluate both the effect of the aggregate size, quantified by the two first moments of the random number of cells per aggregate,  $n_c$  and  $\sigma_c$ , and the effect of the geometrical compactness of the aggregates, described by the mass fractal dimension  $D$ . In this section, the effect of these factors on the frequency dependence of the backscattering coefficient is studied, and an inversion method is proposed to infer aggregation level of porcine red blood cells from experimental backscatter data previously reported in the literature.<sup>6</sup>

#### A. Relation between the backscattering coefficient and the frequency

Figure 3 shows the relation between the backscattering coefficient of diluted porcine blood, computed by the model, and the incident frequency for varying sizes of aggregates ( $D=2$ ,  $\sigma_c/n_c=10\%$ ). The chosen hematocrit was  $H=4.5\%$ . The radius  $a$  of the red cells was  $2.5 \mu\text{m}$ , and the relative impedance mismatch was chosen at 0.11 by taking published values<sup>22</sup> of the compressibilities and densities of the porcine red cells and of the plasma. The speed of sound  $c$  was assumed to be  $1540 \text{ m s}^{-1}$ .

Several features should be noted, depending on the range of frequencies studied.

- At very low frequencies, the red cells in a single aggregate are concentrated in a domain much smaller than the acoustic wavelength and consequently scatter coherently without phase delay. The aggregates can then be considered as single Rayleigh scatterers with an effective volume  $WV_s$ . Since the central positions of the aggregates are spatially Poisson-distributed in the NSP (at this low hematocrit condition), the backscattered power is simply proportional to  $WV_s$ , and thus is sensitive to variations of the number of cells per aggregate. Furthermore, Rayleigh scattering implies that the backscattering coefficient increases proportionally with  $k^4$ , as observed in Fig. 3.
- At very high frequencies, red cells are separated by distances corresponding to many wavelengths. Phases between backscattered echoes are then uniformly distributed between 0 and  $2\pi$  and the structure factor  $S(q)$  becomes 1. The backscattered power is no longer sensitive to the aggregation process but only to the intrinsic properties of the red cells. Figure 3 shows that all curves asymptotically approach this aggregation-independent form. When the frequency reaches  $1.37 \times (c/2\pi a) = 134 \text{ MHz}$  (corresponding to the maximal backscattering cross-section of the red

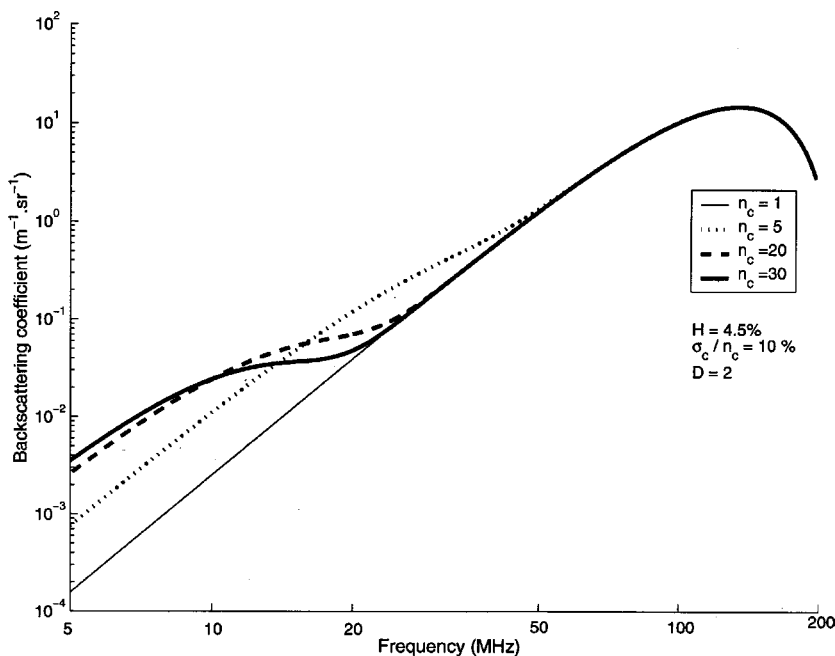


FIG. 3. The backscattering coefficient of porcine blood as a function of the frequency for different aggregation conditions as predicted by the Neyman–Scott modeling.

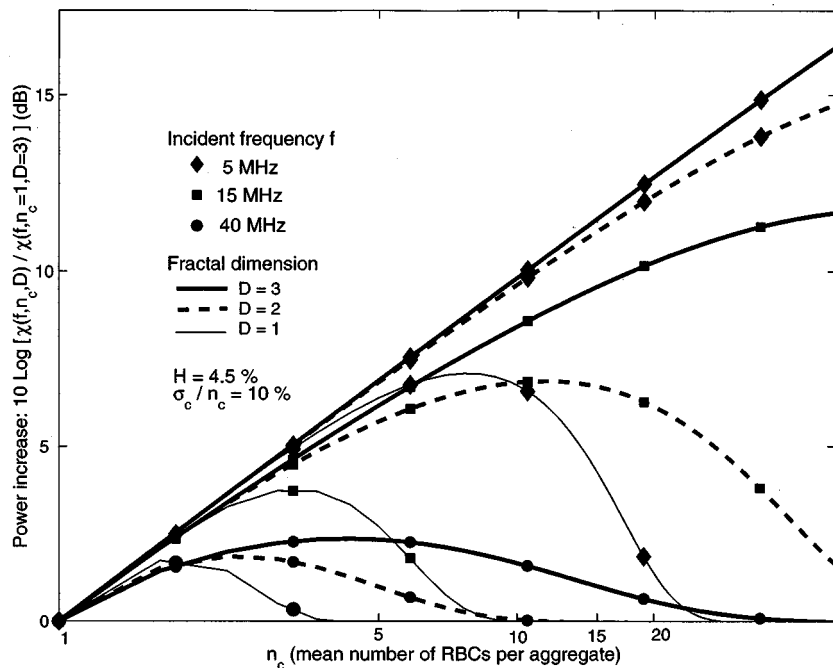


FIG. 4. The backscattered power increase due to the aggregation of red blood cells as predicted by the Neyman–Scott modeling, as a function of the mean number of cells per aggregate  $n_c$ , for different frequencies and fractal dimensions of aggregates. The hematocrit is fixed at  $H=4.5\%$  and the polydispersity is characterized by  $\sigma_c/n_c=10\%$ . The reference power is the disaggregated state, when  $n_c=1$  and  $\sigma_c=0$ .

cell), the backscattering coefficient has a maximal value and then further decreases because of the progressive cancellation of the echoes scattered by the spherical particles. This results from the fact that the wavelets backscattered by boundaries of the particles interfere when the dimensions of the particle are comparable to the wavelength.

- The intermediate frequency range between the two previous scattering regimes is characterized by a decrease of the spectral slope  $\partial \log \chi(k) / \partial \log k$ . When the gyration radius of the aggregates is elevated, the size factor  $\Delta$  decreases. This transition then appears at lower frequencies and is more pronounced when the packing factor  $W$  has a high value. The experimental observation that the frequency dependence decreases in presence of red cell aggregates could be explained by this transitional scattering behavior: non-Rayleigh effects occur more markedly when aggregates are present.

## B. Relation between the backscattering coefficient and the size of aggregates

Figure 4 shows the variations of the backscattering coefficient at three fixed frequencies (5 MHz, 15 MHz and 40 MHz) as a function of the mean number of cells per aggregate and fractal dimension  $D$ . A constant hematocrit  $H=4.5\%$  and a polydispersity characterized by  $\sigma_c/n_c=10\%$  were used for these computations. Results are presented in terms of the power increase (in dB) due to the aggregation in comparison with the disaggregated state [when  $S(q)=1$ ].

The increase in backscattered power due to aggregation is conditioned both by the fractal dimension of the clusters and by the mean number of particles inside the aggregate.

When  $n_c \ll (\lambda/a)^D$ , the power increase is simply proportional to  $n_c$ : the suspension behaves as a collection of bigger particles with size  $\sigma$  that satisfies the Rayleigh hypothesis

$\sigma \ll \lambda$ . Combination of a compact growth of aggregates ( $D \approx 3$ ) and of a low frequency insonification results in this type of scattering.

After this linear increase, the raise in power peaks and is controlled by the unphasing. The higher the frequency, the less pronounced is the relative increase of the backscatter due to aggregation.

A spatial growth of the aggregates, without variation of the number of cells per aggregate, would result in phase differences between echoes coming from the cells of the cluster and thus in a decrease of the backscattered power. On the other hand, an increase of the number of scatterers in the clusters, keeping the aggregate volume constant, increases the scattering strength of each aggregate. These reasons explain why an increase of  $n_c$  has two competitive effects: an increase of the power due to the compaction of the aggregate, and a decrease of the power due to the spatial dilation of the aggregates resulting in incoherent echoes.

Generally, for a fixed number of cells per clusters, the power increase is bigger when the clusters are compact, and thus when  $D$  is closer to 3. The effect of the fractal dimension is more pronounced when the aggregates are bigger.

As shown in Fig. 4, in aggregative conditions, a level of backscattering coefficient ambiguously corresponds to two different values of  $n_c$ . Moreover, the fact that two factors,  $W$  and  $\Delta$ , characterize the NSP, shows that at least two measurements must be accomplished to estimate their values. This therefore suggests that a good characterization of the aggregation phenomenon requires measurements on a large band of frequencies rather than at a single frequency. The following subsection gives a method to extract morphological informations on the aggregates by performing measurements over a whole range of frequencies. This can be technically achieved by using either a broadband transducer that emits short pulses and by making a spectral analysis of the

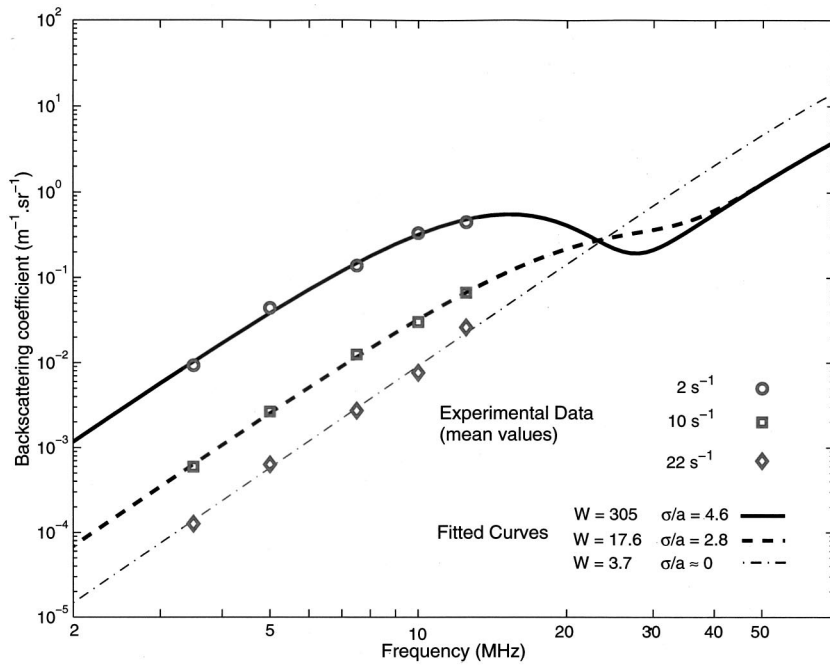


FIG. 5. Experimental backscatter data obtained by Yuan and Shung (Ref. 6) for porcine whole blood flowing at different shear rates, for a hematocrit  $H = 4.5\%$ . Fitted curves are also shown with estimated values of  $W$  (packing factor) and  $\sigma/a$  (normalized radius of the aggregates).

backscattered signal, or by using several transducers with different central frequencies.

### C. Extraction of structural information on the aggregation level from backscattering experiments

In Fig. 5, mean results of backscattering experiments obtained by Yuan and Shung<sup>6</sup> are presented for porcine whole blood, circulating in a laminar shear flow, at a low hematocrit  $H = 4.5\%$ . The *in vitro* model, used by these authors, allowed to control the flow rate inside a cylindrical tube and consequently to modulate the aggregation level of the red cells by changing the mean shear rate. Five different transducers were used to study the frequency dependence of the backscattering coefficient. Mean backscattering coefficients measured for mean shear rates of  $2 \text{ s}^{-1}$ ,  $10 \text{ s}^{-1}$  and  $22 \text{ s}^{-1}$  are shown (the plasmatic fibrinogen concentration, a protein that affects the level of aggregation, was kept constant at  $210 \text{ mg/dl}$  in the three experiments). As expected, at a fixed frequency, the backscattering coefficient decreased when the shear rate increased. The spectral slope is 4 at a shear rate of  $22 \text{ s}^{-1}$  and decreases with decreasing shear rate (a power law fitting between  $3.5 \text{ MHz}$  and  $12.5 \text{ MHz}$  gives a mean spectral slope of 3.7 for  $10 \text{ s}^{-1}$ , and 3 for  $2 \text{ s}^{-1}$ ).

To assess the aggregation state of the red cells for these flowing conditions, a regression method was used to estimate the parameters  $W$  and  $\Delta$ . The analytical expression of the structure factor obtained by the model was fitted to experimental structure factors derived from experimental measurements of backscattering coefficients.

Supposing that the experimental backscattering coefficients  $\{\chi_i\}_{i=1\dots M_f}$  were measured at  $M_f$  different frequencies  $\{f_i\}_{i=1\dots M_f}$ , the corresponding experimental structure factors  $\{S_i\}_{i=1\dots M_f}$  can be computed by using Eq. (2). Noting  $k_i = 2\pi f_i/c$  the sequence of wave numbers, one obtains:

$$S_i = \frac{V_s \chi_i}{H \sigma_b(-2k_i)}$$

with

$$\sigma_b(-2k_i) = \frac{4a^2}{9} (k_i a)^4 \bar{C}^2 \left| 3 \frac{\sin 2k_i a - 2k_i a \cos 2k_i a}{(2k_i a)^3} \right|^2. \quad (19)$$

If the blood sample is characterized by the structure factor  $W$  and the size factor  $\Delta$ , the theoretical structure factors at the same frequencies should be given by Eq. (17):

$$S_i^{\text{theory}} = 1 + (W - 1) \exp\left(-\frac{f_i^2}{2f_0^2} \Delta^{-2}\right), \quad (20)$$

with  $f_0 = c/4\pi a = 49 \text{ MHz}$  for porcine red blood cells.

A nonlinear regression on the parameters  $\{W, \Delta\}$  was performed by minimizing the mean quadratic error  $J(W, \Delta)$  between the theoretical and the experimental values. It is a two variables optimization problem that consists in minimizing a least-square criterion:

$$\begin{aligned} J(W, \Delta) &= \frac{1}{M_f} \sum_i (S_i - S_i^{\text{theory}})^2 \\ &= \frac{1}{M_f} \sum_i (S_i - 1 - (W - 1)e^{-f_i^2/2f_0^2 \Delta^{-2}})^2. \end{aligned} \quad (21)$$

The Nelder–Mead simplex algorithm was used to solve this nonlinear regression problem. The estimates  $\{\hat{W}, \hat{\Delta}\}$  and the minimal value  $J_{\min} = J(\hat{W}, \hat{\Delta})$  correspond to the best prediction error  $J_{\min}^{1/2}$ . The resulting curves of the frequency dependence of the backscattering coefficient appear in Fig. 5.

Table II gives the numerical values of the aggregation parameters obtained by this fitting procedure. The aggregate spatial extent  $\hat{\sigma}$  and the packing factor  $\hat{W}$  are both decreasing

TABLE II. Estimated values of the aggregation parameters corresponding to experimental data obtained by Yuan and Shung (Ref. 6).

Shear rate ( $s^{-1}$ )	$\hat{W}$	$\hat{\Delta}$	$\hat{\sigma}/a$	error $J_{\min}^{1/2}$
2	305	0.31	4.6	21
10	17.6	0.51	2.8	0.8
22	3.7	$+\infty$	0	0.5

with the shear rate. The hypothesis of the disruption of the clusters with an increase of the shear forces is compatible with this tendency.

To reconstitute the aggregate morphology, the three variables  $\{n_c, \sigma_c, D\}$  are required, but the nonlinear regression only supplies two factors. In order to estimate the moments  $n_c$  and  $\sigma_c$  of  $N_c$ , the fractal dimension  $D$  is supposed to be known. The estimated mean number  $\hat{n}_c$  of red cells per aggregate and the polydispersity  $\hat{\sigma}_c$  are computed by using the two relations  $\hat{W} = \hat{n}_c + (\hat{\sigma}_c^2/\hat{n}_c)$  and  $\hat{\Delta} = (1/\sqrt{2})(\hat{n}_c - 1)^{-1/D}$ . Table III gives the resulting values of  $\hat{n}_c$  and  $\hat{\sigma}_c$  for different fractal dimensions. Some fractal dimensions do not always allow the inversion of the relation, which shows that they may not be physically possible. For a shear rate of  $10 s^{-1}$ , e.g.,  $\hat{\sigma}_c^2$  is found negative for  $D=3$ : the aggregates must have a lower fractal dimension than 3. For a high shear rate, the fractal dimension has a low impact because the size of the aggregates remains small.

Three-dimensional realizations of the NSP are generated to visually show the spatial organization of the red cell aggregates (Figs. 6, 7, 8). The random number of cells per aggregate ( $N_c$ ) is supposed to follow a log-normal distribution<sup>23</sup> with the fitted variance and mean. The chosen hematocrit is still 4.5%. For these simulations, we hypothesized that at a shear rate of  $2 s^{-1}$ , the clusters are more compact and thus have a fractal dimension close to 3, whereas that for a shear rate of  $10 s^{-1}$ ,  $D$  is smaller (simulation is generated for  $D=2$ ). When the shear rate is  $22 s^{-1}$ , the fractal dimension does not influence the structure because most of the aggregates are disrupted ( $n_c \approx 1$ ).

#### D. Summary of the basic assumptions of the model, its strengths and limitations

In this study, blood is considered as a medium with weakly varying acoustical properties, as the mismatch between the red blood cell impedance and the plasmatic impedance is only 11%. This allows one to use the Born approximation to relate the frequency-dependent backscattering coefficient to the characteristics of the spatial distribution of acoustical impedance. It was hypothesized that the red blood

TABLE III. First moments (mean  $n_c$  and standard deviation  $\sigma_c$ ) of the size histogram as a function of the mass fractal dimension  $D$  for the models fitted to the experimental data of Yuan and Shung (Ref. 6).

Shear rate ( $s^{-1}$ )	$\hat{n}_c$	$\hat{\sigma}_c$	$\hat{n}_c$	$\hat{\sigma}_c$	$\hat{n}_c$	$\hat{\sigma}_c$
	$D=1$	$D=1$	$D=2$	$D=2$	$D=3$	$D=3$
2	5.6	40.9	22.1	79	98.3	143
10	3.8	7.2	8.8	8.8	23	impossible
22	1	1.6	1	1.6	1	1.6

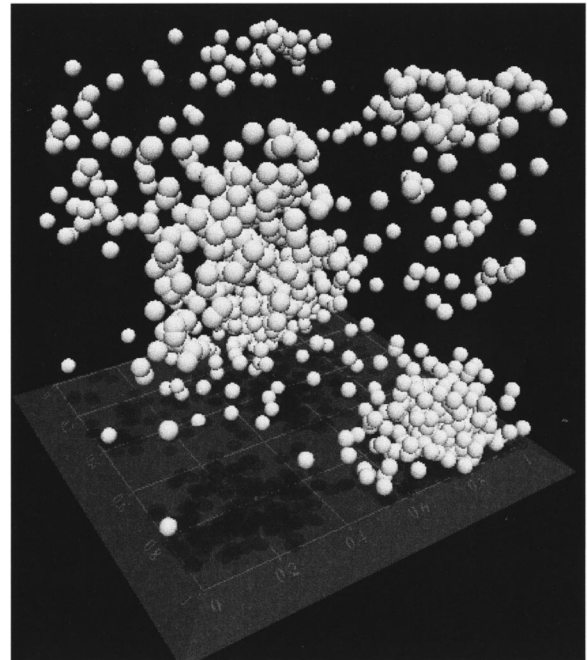


FIG. 6. A realization of the Neyman–Scott process for fitted parameters  $n_c$ ,  $\sigma_c$  and  $\sigma$ , corresponding to experiments with blood flowing at a shear rate of  $2 s^{-1}$  and a hematocrit  $H=4.5\%$ . The fractal dimension  $D$  is 3. The simulation was generated in a cube with dimensions of  $150 \mu\text{m}$ .

cells, that create the fluctuations of impedance, are all similar in shape, and that their relative positioning in the scattering volume results from a stationary random process. The influence of the intrinsic physical properties of the red cells on the backscattering properties of blood is well described by the backscattering cross-section  $\sigma_b$  of a spherical particle in the range of classical imaging frequencies. The influence of

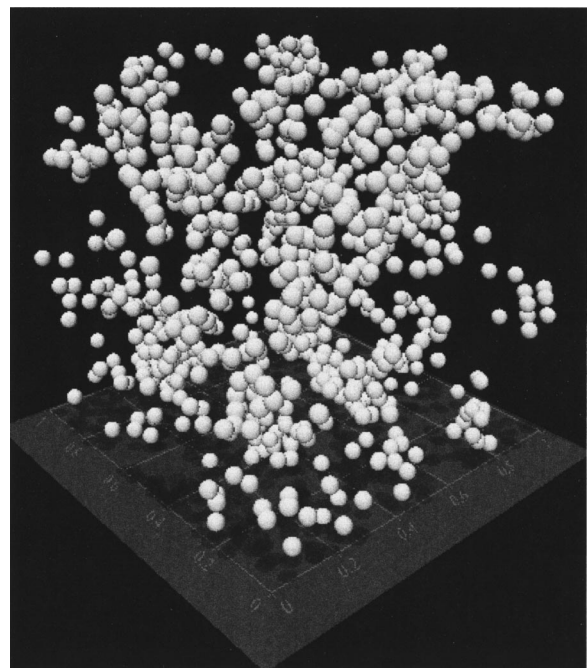


FIG. 7. A realization of the Neyman–Scott process for fitted parameters  $n_c$ ,  $\sigma_c$  and  $\sigma$ , corresponding to experiments with blood flowing at a shear rate of  $10 s^{-1}$  and a hematocrit  $H=4.5\%$ . The fractal dimension  $D$  is 2. The simulation was generated in a cube with dimensions of  $150 \mu\text{m}$ .

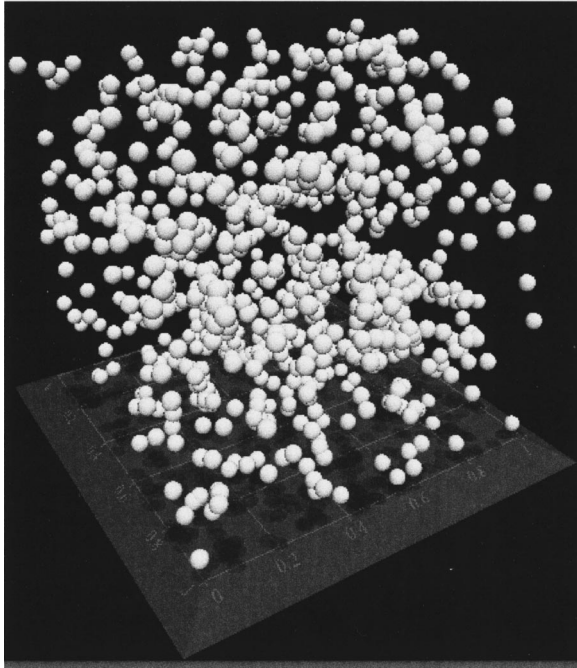


FIG. 8. A realization of the Neyman–Scott process for fitted parameters  $n_c$ ,  $\sigma_c$  and  $\sigma$ , corresponding to experiments with blood flowing at a shear rate of  $22 \text{ s}^{-1}$  and a hematocrit  $H=4.5\%$ . The fractal dimension  $D$  is 1. The simulation was generated in a cube with dimensions of  $150 \mu\text{m}$ .

the red cell aggregation level is investigated by modeling the spatial density  $N(\mathbf{x})$  of the red cell positions by the Neyman–Scott point process. The complexity of modeling  $N(\mathbf{x})$  in physiological conditions comes from two reasons. First, the high density of the red cells (about  $5 \times 10^6 \text{ mm}^{-3}$ ), representing a normal hematocrit around 45%, imposes important restrictions on the random positioning of the red cells because of their nonoverlapping. Second, the reversible aggregation process favors the creation of groups of red cells with varying morphologies. The NSP provides a statistical description of the aggregates by characterizing their number of cells and their spatial extent. The main advantage of the NSP is the fact that it allows the analytical computation of the Fourier spectrum of  $N(\mathbf{x})$ , which directly gives the frequency dependent structure factor. It gives a parametric model to the frequency dependence of backscatter experimental data, and provides meaningful morphological features of the aggregates ( $\{W, \Delta\}$  or  $\{n_c, \sigma_c\}$  when the fractal dimension  $D$  is known), that are more physically relevant for blood characterization than the absolute value of the backscattering coefficient or the spectral slope.

However, the simplicity of the NSP has a drawback: constraints imposed by the high hematocrit behavior are not taken into consideration. Equation (18) shows that the backscattering coefficient evolves linearly with the hematocrit when the medium is described by the NSP. But it is known, when the hematocrit is greater than a few percents, that the ultrasonic backscatter of blood tends to decrease. For nonaggregating red blood cells ( $n_c=1$  and  $\sigma_c=0$ ), the value of the packing factor predicted by the NSP is 1, whereas in this case  $W$  was shown<sup>12,24</sup> to be hematocrit-dependent [for spherical hard scatterers, the three-dimensional Percus–Yevick approximation yields  $W \approx (1-H)^4/(1+2H)^2$ ]. This

nonlinear relation between the hematocrit and the backscattering coefficient cannot be predicted by the NSP. Moreover, the NSP generates clusters of points that allows cells overlapping. When the medium is dense, this results in unrealistic realizations. Experimentally, the linear relationship between the backscattering coefficient and the hematocrit was shown valid<sup>25</sup> up to  $H \approx 5\%$ . One can therefore consider that the NSP is appropriate to model red cell aggregate configurations for a hematocrit under 5%.

Despite these limitations, these results could be clinically valuable in hematological laboratories to study the erythrocyte aggregability for blood sample adjusted to a fixed low hematocrit. *In vitro* scattering measurements with diluted red cell suspensions can provide flow dependence of  $\{W, \Delta\}$ , and would characterize the intrinsic properties of red cells to aggregate. It may be of interest to note that optical microscopic observations<sup>26</sup> of red cell aggregates, already used in research laboratories, are also performed at these low hematocrits for adequate morphological measurements.

One fundamental interest of the Neyman–Scott model was to distinguish intrinsic effects of the aggregation level on the backscattering from the effect of hematocrit. Non-Rayleigh effects associated with the growth of the gyration radius of the aggregates were related to the frequency dependence of the backscattering coefficient. However, to apply inference techniques to blood characterization with more physiological hematocrits (around 45%) to predict physical parameters describing the aggregation process, spatial stochastic processes that can both describe dense and aggregative media will have to be studied for modeling red cell positioning. Unfortunately, more complex estimation techniques are required to characterize them because spectral properties of such random processes may not be analytically calculated.

## V. CONCLUSION

Ultrasound backscattering properties of blood are dependent on the packing state of the red cells. It would be of interest to use this dependence to quantitatively measure the erythrocyte aggregation level by acoustical means. To reach this goal, a clear understanding of the relation existing between the variables describing the aggregation state and the backscatter data must be found. Most of the previous theoretical studies intended to clarify the hematocrit-dependence of the backscattering, or concerned low frequency backscattering by non-Rayleigh red cell aggregates. However, the influence of the aggregation level on the frequency dependence of the backscattering was not directly addressed whereas experimental results showed that at a low shear rate, aggregates of red cells cannot be considered as Rayleigh scatterers even at low frequencies.

To extend scattering theory to aggregating red cell suspensions, the spatial pattern due to the clustering was modeled by a random process. Considering that the erythrocyte positioning is the realization of a Neyman–Scott process, and using the Born approximation, the structure factor of a low hematocrit ( $H < 5\%$ ) but aggregative suspension of red blood cells was predicted analytically, as a function of the size distribution of the aggregates and of their mass fractal

dimension. This probabilist framework conveyed a parametric model to extract the average size of the clusters of red cells and its polydispersity from backscatter data, assuming that the mass fractal dimension is known. Experimental measurements on a 4.5% hematocrit porcine blood obtained by Yuan and Shung<sup>6</sup> were used to test the efficiency of the model. The disaggregation of the groups of red cells and the decrease of the polydispersity, both associated with an increase of the shear rate, could be determined by a regression technique.

The NSP represents a first step to the random modeling of the microstructural organization of red blood cells, that helps to understand the frequency dependence of the backscattering properties of blood due to aggregation. It must be emphasized that  $S(q)$ , the structure factor, is a crucial quantity to determine for blood characterization. It reflects the organization of the red cell network, equivalently to the pair correlation function. The zero-frequency limit of the structure factor, the packing factor  $W$ , is useful to describe low frequency scattering (Rayleigh scattering). However, low frequency measurements only give limited structural informations, as Bascom and Cobbold pointed out,<sup>10</sup> because the packing factor  $W$  does not uniquely define the pair correlation function as the structure factor does. A spatial random model, as the NSP, allows us to characterize the spectral variations of the structure factor of a low hematocrit suspension by a small number of variables. This kind of parametric approach reveals particularly useful when considering the experimental difficulties in reliably measuring backscattering coefficients of materials.<sup>27</sup> Substantial *a priori* knowledge of the frequency dependence is expected to compensate for the uncertainties of the measurements. The NSP highlighted two factors as the structure factor  $W$  and the size factor  $\Delta$ , themselves related to meaningful geometrical properties of the red cell aggregates. For high hematocrits and aggregative suspensions, an appropriate model still remains to be found, to discriminate such significant factors and to use them as clinical indices of red cell aggregation.

## ACKNOWLEDGMENTS

We wish to thank Isabelle Fontaine for many helpful discussions and for reviewing the manuscript. This work was supported by the following grants: Studentship from the "Groupe de recherche en modélisation biomédicale" of the Institute of Biomedical Engineering of the École Polytechnique and Université de Montréal; Scholarship from the "Fonds de la recherche en santé du Québec;" Grants from the Medical Research Council of Canada (# MOP-36467)—now the Canadian Institutes of Health Research—and the Heart and Stroke Foundation of Québec.

<sup>1</sup>G. D. O. Lowe, "Agents lowering blood viscosity, including defibrinating agents," in *Cardiovascular Thrombosis: Thrombocardiology and Thromboneurology*, 2nd ed., edited by M. Verstraete, V. Fuster, and E. J. Topol (Lippincott-Raven, Philadelphia, 1998), Chap. 18, pp. 321–333.

<sup>2</sup>W. Koenig and E. Ernst, "The possible role of hemorheology in atherothrombogenesis," *Atherosclerosis (Berlin)* **94**, 93–107 (1992).

<sup>3</sup>Z. Vered, G. A. Mohr, B. Barzilai, C. J. Gessler, S. A. Wickline, K. A. Wear, T. A. Shoup, A. N. Weiss, B. E. Sobel, and J. G. Miller, "Ultrasound integrated backscatter tissue characterization of remote myocardial infarction in human subjects," *J. Am. Coll. Cardiol.* **13**, 84–91 (1989).

<sup>4</sup>S. Takiuchi, H. Rakugi, K. Honda, T. Masuyama, N. Hirata, H. Ito, K. Sugimoto, Y. Tanagitani, K. Moriguchi, A. Okamura, J. Higaki, and T. Ogihara, "Quantitative ultrasonic tissue characterization can identify high-risk atherosclerotic alteration in human carotid arteries," *Circulation* **102**, 766–770 (2000).

<sup>5</sup>P. Stetson and G. Sommer, "Ultrasonic characterization of tissues via backscatter frequency dependence," *Ultrasound Med. Biol.* **23**, 989–996 (1997).

<sup>6</sup>Y. W. Yuan and K. K. Shung, "Ultrasonic backscatter from flowing whole blood: II. Dependence on frequency and fibrinogen concentration," *J. Acoust. Soc. Am.* **84**, 1195–1200 (1988).

<sup>7</sup>F. S. Foster, H. Obara, T. Bloomfield, L. K. Ryan, and G. R. Lockwood, "Ultrasound backscatter from blood in the 30 to 70 MHz frequency range," *IEEE Ultrasonics Symposium Proceedings* 1599–1602 (1994).

<sup>8</sup>M. S. van der Heiden, M. G. de Kroon, N. Bom, and C. Borst, "Ultrasound backscatter at 30 MHz from human blood: Influence of rouleau size affected by blood modification and shear rate," *Ultrasound Med. Biol.* **21**, 817–826 (1995).

<sup>9</sup>V. Twersky, "Low frequency scattering by correlated distributions of randomly oriented particles," *J. Acoust. Soc. Am.* **81**, 1609–1614 (1987).

<sup>10</sup>P. A. Bascom and R. S. Cobbold, "On a fractal packing approach for understanding ultrasonic backscattering from blood," *J. Acoust. Soc. Am.* **98**, 3040–3049 (1995).

<sup>11</sup>L. Y. Mo and R. S. Cobbold, "A unified approach to modeling the backscattered Doppler ultrasound from blood," *IEEE Trans. Biomed. Eng.* **39**, 450–461 (1992).

<sup>12</sup>I. Fontaine, M. Bertrand, and G. Cloutier, "A system-based approach to modeling the ultrasound signal backscattered by red blood cells," *Biophys. J.* **77**, 2387–2399 (1999).

<sup>13</sup>B. G. Teh and G. Cloutier, "Modeling and analysis of ultrasound backscattering by spherical aggregates and rouleaux of red blood cells," *IEEE Trans. Ultrason. Ferroelectr. Freq. Control* **47**, 1025–1035 (2000).

<sup>14</sup>P. M. Morse and K. U. Ingard, *Theoretical Acoustics* (Princeton University Press, Princeton, NJ, 1986).

<sup>15</sup>M. F. Insana and D. G. Brown, "Acoustic scattering theory applied to soft biological tissues," in *Ultrasonic Scattering in Biological Tissues*, edited by K. K. Shung and G. A. Thieme (CRC, Boca Raton, FL, 1993), Chap. 5, pp. 75–124.

<sup>16</sup>N. E. Berger, R. J. Lucas, and V. Twersky, "Polydisperse scattering theory and comparisons with data for red blood cells," *J. Acoust. Soc. Am.* **89**, 1394–1401 (1991).

<sup>17</sup>J. Serra, *Image Analysis and Mathematical Morphology* (Academic, London, 1982).

<sup>18</sup>J. L. F. Batista and D. A. Maguire, "Modeling the spatial structure of tropical forests," *Forest Ecology & Management* **110**, 293–314 (1998).

<sup>19</sup>J. Caers, "A general family of counting distributions suitable for modeling cluster phenomena," *Math. Geol.* **28**, 601–624 (1996).

<sup>20</sup>B. Bacchi, R. Ranzi, and M. Borga, "Statistical characterization of spatial patterns of rainfall cells in extratropical cyclones," *J. Geophys. Res. [Atmos.]* **101**, 26277–26286 (1996).

<sup>21</sup>M. Elimelech, J. Gregory, X. Jia, and R. A. Williams, *Particle Deposition & Aggregation. Measurement, Modeling and Simulation* (Butterworth-Heinemann, Woburn, MA, 1995).

<sup>22</sup>Y. W. Yuan and K. K. Shung, "Ultrasonic backscatter from flowing whole blood: I. Dependence on shear rate and hematocrit," *J. Acoust. Soc. Am.* **84**, 52–58 (1988).

<sup>23</sup>K. W. Lee, "Change of particle size distribution during Brownian coagulation," *J. Colloid Interface Sci.* **92**, 315–325 (1983).

<sup>24</sup>V. Twersky, "Acoustic bulk parameters in distributions of pair-correlated scatterers," *J. Acoust. Soc. Am.* **64**, 1710–1719 (1978).

<sup>25</sup>L. Y. L. Mo, I. Y. Kuo, K. K. Shung, L. Ceresne, and R. S. C. Cobbold, "Ultrasound scattering from blood with hematocrits up to 100%," *IEEE Trans. Biomed. Eng.* **41**, 91–95 (1994).

<sup>26</sup>S. Chen, B. Gavish, S. Zhang, Y. Mahler, and S. Yedgar, "Monitoring of erythrocyte aggregate morphology under flow by computerized image analysis," *Biorheology* **32**, 487–496 (1995).

<sup>27</sup>E. L. Madsen, F. Dong, G. R. Frank, B. S. Garra, K. A. Wear, T. Wilson, J. A. Zagzebski, H. L. Miller, K. K. Shung, S. H. Wang, E. J. Feleppa, T. Liu, W. D. O'Brien, Jr., K. A. Topp, N. T. Sanghvi, A. V. Zaitsev, T. J. Hall, J. B. Fowlkes, O. D. Kripfgans, and J. G. Miller, "Interlaboratory comparison of ultrasonic backscatter, attenuation, and speed measurements," *J. Ultrasound Med.* **18**, 615–631 (1999).